Title

The effects of damage accumulation in optimizing a piezoelectric energy harvester configuration

Authors

Kjolsing, Eric J
Todd, Michael D

Publication Date

2018-03-27

DOI

10.1117/12.2283053

Peer reviewed

The effects of damage accumulation in optimizing a piezoelectric energy harvester configuration

Eric J. Kjolsing*[a], Michael D. Todd[b]
[a]Structural Integrity Associates, Inc., 9710 Scranton Road, San Diego, CA, USA, 92121; [b]Dept. of Structural Engineering, University of California San Diego, 9500 Gilman Drive, La Jolla, CA, USA, 92093

ABSTRACT

Bimorph piezoelectric elements are often used to harvest energy for low-power structural health monitoring systems. When these piezoelectric elements are deployed for extended periods of time and operate under near-resonant conditions, the resulting high amplitude cycling can lead to degradation of the piezoelectric element, resulting in a shift in the design fundamental frequency. For scenarios in which the piezoelectric harvester is subject to slowly-varying time-dependent frequency inputs, the natural frequency shift due to degradation may cause the piezoelectric harvester to detune from resonance, subsequently affecting the harvester's power output. The current study seeks to understand how the accumulation of damage shifts the optimal tip mass and resistive load in a bimorph piezoelectric energy harvester. A cantilever piezoelectric element is modeled utilizing coupled electromechanical equations in a distributed system. The piezoelectric is subject to ground accelerations; the resulting power output is recorded for a range of tip masses and resistive loads. A rainflow analysis is then performed to calculate the piezoelectric element's tip displacement amplitude and the corresponding cycle count. A damage accumulation model based on a weighted form of Miner's rule is then used to degrade the harvester's flexural rigidity, piezoelectric capacitance, and piezoelectric strain constant. The piezoelectric is again loaded and the process repeated. The resulting power output contours reveal how the optimal realization of tip mass and resistive load changes as damage accumulates in the piezoelectric element. Apparent trends in the power output contours are explained. Approved for publication, LA-UR-18-20075.

Keywords: piezoelectric energy harvesting, damage accumulation, rainflow analysis, structural health monitoring

1. BACKGROUND

The hydrocarbon industry has a stated interest in developing energy harvesting and storage systems for downhole deployment to supplement currently utilized power sources. Several investigations were previously performed to forward this objective [1]-[4]. Since long deployment cycles are desirable, the selection of an optimal harvester configuration must account for long-term effects, specifically the accumulation of damage. "Optimal" in the present discussion refers to a maximization of power output over a specific duration.

The objective of the current study is to observe how damage accumulation affects the selection of optimal tip mass and resistive load in a piezoelectric bimorph. To achieve this objective, this manuscript presents four analytical cases with varying damage scenarios and compares the dynamic characteristics and power output between them.

2. PIEZOELECTRIC MODEL

A single piezoelectric bimorph is modeled utilizing coupled electromechanical equations for a distributed system. The model's derivation is provided by Erturk and Inman [5] with the final result presented here. The model has been experimentally validated and is discussed by others [6, 7]. The same modeling approach has been applied to a unimorph piezoelectric element [6, 8]; for additional details, the reader is referred to Erturk and Inman [5].

Consider a driving harmonic base motion of the form

$$w_b = \bar{W}_B e^{i\omega t}, \tag{1}$$

where $\bar{W}_B$ is the translation amplitude and ω is the excitation frequency. It can be shown that the steady state output voltage (v) can be related to the base acceleration ($\ddot{w}_B$) through a frequency response function (α) as

$$v = \alpha \ddot{w}_B. \tag{2}$$

The frequency response function (FRF) has been shown to be

$$\alpha(\omega) = \frac{-\sum_{r=1}^{\infty} \frac{\Theta_r i\omega\sigma_r}{(-\omega^2 + 2\zeta_r\omega_r i\omega + \omega_r^2)}}{\frac{i\omega\Theta_r^2}{\sum_{r=1}^{\infty}(-\omega^2 + 2\zeta_r\omega_r i\omega + \omega_r^2)} + \left[C_{\tilde{p}}^{eq} i\omega + \frac{1}{R}\right]}, \tag{3}$$

where the variables include the mode number (r), the modal electromechancial coupling term (Θ_r), the modal damping ratio (ζ_r), the undamped natural frequency (ω_r), the equivalent capacitance for the piezoelectric bimorph ($C_{\tilde{p}}^{eq}$), and the circuits resistive load (R). The forcing function coefficient (σ_r) is written as

$$\sigma_r = -m\int_0^L \phi_r dx - M_t\phi_r(L), \tag{4}$$

where the variables include the piezoelectric beam mass per unit length (m), eigenfunction (ϕ_r), and tip mass (M_t). Similarly, a FRF relating the relative displacement (w_R) to the base acceleration can be written as

$$w_R = \beta \ddot{w}_B, \tag{5}$$

where

$$\beta(\omega, x) = \sum_{r=1}^{\infty} \left\{ \sigma_r - \Theta_r \frac{\sum_{r=1}^{\infty} \frac{\Theta_r i\omega\sigma_r}{(-\omega^2 + 2\zeta_r\omega_r i\omega + \omega_r^2)}}{\frac{i\omega\Theta_r^2}{\sum_{r=1}^{\infty}(-\omega^2 + 2\zeta_r\omega_r i\omega + \omega_r^2)} + \left[C_{\tilde{p}}^{eq} i\omega + \frac{1}{R}\right]} \right\} \frac{\phi(x)}{(-\omega^2 + 2\zeta_r\omega_r i\omega + \omega_r^2)}. \tag{6}$$

The model can be expanded to account for periodic loading using a Fourier series approximation of the driving motion [5]. This leads to

$$v(t) = \sum_{n=1}^{N} \left|\alpha\left(n\frac{2\pi}{T}\right)\right| \left[a_n \cos\left[\left(n\frac{2\pi}{T}t\right) + \Phi\left(n\frac{2\pi}{T}\right)\right] + b_n \sin\left[\left(n\frac{2\pi}{T}t\right) + \Phi\left(n\frac{2\pi}{T}\right)\right]\right], \tag{7}$$

where $|\alpha(2\pi n/T)|$ and $\Phi(2\pi n/T)$ are the modulus and phase angle of the FRF α, a_n and b_n are Fourier series coefficients, and T is the signal length. Similarly, the relative displacement response can be found as

$$w_R(x,t) = \sum_{n=1}^{N} \left|\beta\left(n\frac{2\pi}{T}\right)\right| \left[a_n \cos\left[\left(n\frac{2\pi}{T}t\right) + \Psi\left(n\frac{2\pi}{T}\right)\right] + b_n \sin\left[\left(n\frac{2\pi}{T}t\right) + \Psi\left(n\frac{2\pi}{T}\right)\right]\right]. \tag{8}$$

The instantaneous power output is written as

$$P_{inst}(t) = \frac{v(t)^2}{R}. \tag{9}$$

The average power output is then

$$P_{avg} = \frac{1}{T}\int_0^T P_{inst}(t)dt. \tag{10}$$

3. DAMAGE ACCUMULATION MODEL

System properties are known to degrade when the system is subjected to repeated load cycles. For example, the accumulation of microcracking in the bimorph will cause a decrease in its flexural rigidity. This will lead to a change in the system's natural frequency and may result in detuning from resonance, directly impacting the power output. To account for such changes, a damage metric and a damage model are needed.

One common damage metric is stress: a representative element is cycled at a constant stress level until failure with element properties (e.g. effective flexural rigidity) observed throughout the course of testing. The results are often plotted as property vs. cycles and for multiple tests, stress vs. cycles to failure. This metric becomes difficult to incorporate in conjunction with the utilized piezoelectric model as the relative displacement output from the model (w_R) is based on a spatially uniform (or average) flexural rigidity. While the beam curvature (and subsequently a stress term) can be calculated from this output, the output cannot account for any local damage (i.e., amplified curvature) that might be occurring - this is analogous to a linear analysis failing to capture localized curvature in the plastic hinge of a column.

An alternative metric is the relative tip displacement of the beam ($w_R(x = L)$): rather than cycling a test element to a specified stress level, the element can be cycled to a specified displacement amplitude. As before, element properties can be observed throughout the course of testing and plotted as property vs. cycles and for multiple tests, amplitude vs. cycles to failure.

Consider the testing of Q identical piezoelectric bimorphs with each bimorph subject to a harmonic base acceleration resulting in a relative tip displacement amplitude A_k ($k = 1{:}\,Q$). After n cycles the cyclic loading is stopped and the relevant properties (V^a, V^b, etc.) of each bimorph measured. The Q bimorphs are again cyclically loaded and the process repeated until a property of interest degrades to failure after N cycles. Since the cycles to failure may differ between each amplitude A_k, the reader may find N_k a preferable notation. A graphic depicting this process is shown in Figure 1.

For a given property V with initial value V_i a representative output is enlarged in Figure 2. The degradation to property V after n cycles at amplitude A_k is ΔV_k. Assume the cyclic degradation is linearly additive such that

$$\Delta V_1 + \Delta V_2 + \Delta V_Q = \sum_{k=1}^{Q} \Delta V_k = C * V_i, \tag{11}$$

where C is a damage index representing the percent accumulated degradation of variable V. Eq. (11) can be rewritten as

$$\sum_{k=1}^{Q} \frac{\Delta V_k}{V_i} = C \leq 1, \tag{12}$$

which is seen to be a weighted form of Miner's rule [9]. The value of property V after accumulating damage C is written as

$$V_{damaged} = (1 - C)V_i. \tag{13}$$

4. RAINFLOW ANALYSIS

For non-harmonic motion, a rainflow analysis is performed to determine the amplitude/cycle count necessary to implement the damage model from Section 3. Utilizing a relative tip displacement time history, the rainflow analysis counts the number of equivalent cycles for a range of amplitudes. The test amplitudes (i.e. the A_k's) are used to silo the rainflow output and the cycles falling within each amplitude bin are counted. These cycle counts are then added to the cumulative cycle counts from all previous loading enabling property degradation per Section 3. This process is depicted in Figure 3. The rainflow analysis is performed with the MATLAB toolbox RAINFLOW [10]-[11] for the current investigation.

5. DEMONSTRATION CASES

A piezoelectric configuration is analyzed to determine the optimal tip mass and resistive load over 0.9 years of deployment. The model loading schedule and inputs are shown in Table 1 and Table 2, respectively. The configuration is first analyzed without accounting for damage to develop a baseline result. The configuration is then analyzed accounting for damage to the (i) mechanical terms, (ii) the piezoelectric terms, and (iii) both the mechanical and piezoelectric terms. Apparent trends in the power output contours are explained.

Table 1. Loading schedule.

Start Time (year)	Loading Regime	Loading Amplitude (m/s^2)	Loading Frequency (Hz)	Loading Frequency (rad/s)	End Time (year)
0	1	2	20	125.66	0.3
0.3	2		30	188.50	0.6
0.6	3		25	157.08	0.9

Table 2. Inputs.

Length L, (m)	0.030
Width b, (m)	0.005
Distance to Neutral Axis $\frac{h_{\tilde{p}}+h_{\tilde{s}}}{2}$, (m)	$1e-4$
Modes Considered	1
Damping Ratio	0.010
Tip Mass M_t, (kg)	Optimized Variable
Tip Mass Density ρ_t (kg/m^3)	6000
Tip Inertia I_t, (kgm^2)	Varies, $I_t = \frac{5}{12}\frac{M_t^2}{\rho_t b}$
Damage Index C	Varies
Beam Mass m, (kg/m)	0.02
Operating Temperature (℃)	Constant Temp.
Flexural Rigidity YI, (Nm^2)	$1.090e-3$ & Varies
Piezoelectric Elastic Modulus c_{11}^E, (N/m^2)	$61e9$
Piezoelectric Constant d_{31}, (m/V)	$-171e-12$ & Varies
Piezoelectric Capacitance $C_{\tilde{p}}$, (F)	$1.33e-8$ & Varies
Piezoelectric Configuration	Series
Resistive Load R, (Ω)	Optimized Variable

5.1 Optimal realization for undamaged configuration

Damage is not included in this baseline case (i.e. $C = 0$ for all realizations). For each loading regime the maximum relative tip displacement (MRTD) and average power output are calculated over a range of tip masses and resistive loads. The results are presented in Figure 4 and Figure 5.

For low resistive loads (i.e. $R \approx 0\Omega$, short-circuit condition) the MRTD approaches that of the electromechanically uncoupled system where a maximum response is seen as the undamped natural frequency (ω_r) and the loading frequency converge. As the resistive load is increased, the system shifts from a short-circuit to open-circuit condition, leading to a shift in the system's resonant frequency. The introduction of a resistive load results in piezoelectric power generation and power dissipation in the resistor due to Joule heating [5]. Unlike viscous damping, the observed frequency shift, which is due to the changing electrical boundary condition (i.e. an increased resistive load), causes an upward frequency shift. For the current scenario (where the loading frequency is specified), as the systems resonant frequency increases due to changing resistance the tip mass that maximizes the displacement response must increase (thereby lowering the resonant frequency) such that the resonant frequency and loading frequency coincide. This upwards shift in optimal tip mass is apparent in each plot of Figure 4.

To determine the optimal tip mass and resistive load that maximizes the average power output over all three loading regimes (i.e. from year 0 to 0.9), the average power output from each realization for each loading regime (given in Figure 5) is integrated over the regimes duration resulting in a scalar value that can be used as an optimization metric. The resulting metric is plotted in Figure 6. The total average power output is found to be maximized when $M_t = 0.0066kg$, $R = 5e6\Omega$ and results in an average power output of $1.14mW$, $1.14\mu W$, and $5.56\mu W$ for loading regime one, two, and three, respectively. Note that this realization produces over 99% of its total average power output during the first loading regime due to resonant behavior. The corresponding MRTDs are $2.64mm$, $0.08mm$, and $0.18mm$.

5.2 Optimal realization for damaged configuration

The analysis is repeated while including the linear cumulative damage model described in Section 3. The loading schedule and inputs from Table 1 and Table 2 are unchanged. Since damage accumulation is dependent on load cycles which accumulate over time, the analysis must be discretized in time: the time discretization used in this analysis is $0.05yr$ (although results are often given in coarser increments due to manuscript length restrictions). The mechanical

and electrical terms are first investigated separately to demonstrate their individual effects. Following this, their combined effects are demonstrated as an optimal tip mass and resistive load are selected.

5.2.1 Degradation of flexural rigidity during the first loading regime

The degradation of flexural rigidity is based on load cycling data shown in Figure 7; arbitrary values have been used. The piezoelectric terms are held constant and are assumed not to degrade.

The MRTD and the cumulative damage to the flexural stiffness are plotted in Figure 8 for various tip masses and resistive loads. As damage accumulates, the flexural stiffness of the system is reduced. This results in a decrease in the systems resonant frequency. Since the driving frequency is fixed ($20Hz$ in the first loading regime) the tip mass maximizing the MRTD (i.e. the tip mass corresponding to the largest MRTD) must be reduced as damage is accumulated, thereby offsetting the reduction in system stiffness. This trend is visible in Figure 8 where the tip mass maximizing the MRTD is seen to shift downwards over time (or more accurately, as cyclic damage accumulates). Since the maximum MRTD now occurs for a new (and smaller) tip mass realization, damage will accumulate to a greater degree at the new tip mass realization during the next loading cycle. This can be seen in the damage contours of Figure 8 where damage is seen to accumulate for smaller tip masses in each subsequent time increment.

A second visible trend in Figure 8 is the reduction in the maximum MRTD as the tip mass decreases. This trend is explained by Figure 9 which plots FRFs for the relative tip displacement (assuming constant stiffness). Note that: (1) for a fixed resistive load the magnitude of the displacement FRF decreases with decreasing tip mass, (2) as the tip mass decreases the resonant frequency of the system increases, and (3) as the resistive load increases the resonant frequency of the system increases.

The average power output is shown in Figure 10 where the trends seen in the MRTD contours of Figure 8 are visible. The downward shift in tip mass corresponding to the maximum average power output can again be attributed to damage accumulation. As damage is accumulated, the flexural stiffness of the system is reduced. This results in a decrease in the systems resonant frequencies. Since the driving frequency is fixed ($20Hz$ in the first loading regime) the tip mass maximizing the average power output must be reduced as damage is accumulated, thereby offsetting the reduction in system stiffness.

5.2.2 Degradation of piezoelectric terms during the first loading regime

The degradation of the piezoelectric terms (d_{31} and $C_{\tilde{p}}$) are based on load cycling data shown in Figure 7; arbitrary values have been used. The flexural rigidity is held constant and assumed not to degrade.

The MRTD is plotted in Figure 11 for various tip masses and resistive loads. The cumulative damage to each piezoelectric term is plotted in Figure 12. As noted by the relatively unchanging optimal tip mass in Figure 11, the degradation of the piezoelectric terms is seen to have a significantly smaller impact on the shift of resonance frequency as compared to the degradation of flexural rigidity. This leads to damage being concentrated in those realizations with high relative MRTD. In other words, damage to the piezoelectric terms is localized where the MRTD is high and the realizations for which the MRTD are high are relatively constant.

As previously noted, for low resistive loads the MRTD approaches that of the electromechanically uncoupled system where a maximum response is seen as the undamped natural frequency and the loading frequency converge. Under the short-circuit condition, then, degradation of the piezoelectric terms has a small impact on the MRTD as the system is dominated by the governing mechanical equations. For high resistive loads (e.g. open-circuit condition), the shift in resonance frequency is due to the inclusion of the governing electrical equations. When the piezoelectric terms degrade, the induced shift in the resonant frequency will once again shift (back towards a mechanically governed system) causing a change in the optimal tip mass. These trends can be seen in Figure 11: the MRTD is relatively constant for low resistive loads while for high resistive loads, damage to the piezoelectric terms results in a slight downward shift in the tip mass maximizing the MRTD.

The average power output is also shown in Figure 11. Note that damage to the piezoelectric terms is based on the MRTD and, for the investigated cases, the realizations with high MRTD do not overlap with realizations with high average power output. This means that realizations with significant damage do not coincide with realizations with high average power output (compare Figure 11 and Figure 12). This results in the average power output appearing relatively constant through each time increment.

5.2.3 Combined degradation over all three loading regimes

All three degradation models (Figure 7) are included in a final analysis covering all three loading regimes (recall Table 1). The resulting MRTD and average power contours are shown in Figure 13. The trends identified in 5.2.1 and Section 5.2.2 are apparent in all three loading regimes. The downward shift of tip mass (corresponding to maximum response) between each loading regime is due to the changing loading frequency between each regime: as the loading frequency changes ($20Hz$, $30Hz$, $25Hz$) the tip mass corresponding to resonant behavior changes.

Two interesting results are seen in the damage contours shown in Figure 14 and Figure 15. First, since the degredation of flexural rigidity causes a noticeable shift in the tip mass corresponding to maximum response, degradation of the piezoelectric terms is seen to spread to other tip mass realizations to a greater degree (unlike the concentrated damage shown in Figure 12). Second, damage accumulation is stratified and, for the inputs considered, shows little overlap between each loading regime. As a physical example consider two different tip mass realizations: the first corresponds to a resonant frequency around $20Hz$ (e.g. $M_t \approx 0.0062kg$) while the second corresponds to a resonant frequency around $30Hz$ (e.g. $M_t \approx 0.003kg$). During the first loading regime the first realization is excited near resonance, resulting in relatively significant damage accumulation, while the second realization is not near resonance, resulting in relatively little damage accumulation. During the second loading regime the shift in loading frequency results in the second realization being excited near resonance while the first realization is no longer excited near resonance. Thus, during the second loading regime the additive damage to the first realization is small while the additive damage to the second realization is large. This explains the stratified nature of the damage and its evolution over time/cyclic loading.

To determine the tip mass and resistive load that maximizes the average power output over all three loading regimes (i.e. from year 0 to 0.9), the average power output from each realization is integrated over each time step and summed, resulting in a scalar value that can be used as an optimization metric. The resulting metric is plotted in Figure 16. The total average power output is found to be maximized when $M_t = 0.0062kg$, $R = 1e6\Omega$. The average power output and corresponding MRTD are shown in Figure 17. For comparison purposes, Figure 17 also includes the average power output and corresponding MRTD for (1) the maximized result found in the undamaged case ($M_t = 0.0066kg$, $R = 5e6\Omega$) and (2) the same realization ($M_t = 0.0066kg$, $R = 5e6\Omega$) but when damage is incorporated. When degradation is included in the analysis the power output from the originally optimal realization ($M_t = 0.0066kg$, $R = 5e6\Omega$) drops off rapidly due to a shift in the resonance frequency (i.e. the large initial MRTD leads to significant damage during the first time step which leads to a larger frequency shift in the next time step). The new optimal realization ($M_t = 0.0062kg$, $R = 1e6\Omega$) is seen to accumulate less damage (note the smaller initial MRTD) resulting in a smaller shift of the resonant frequency away from the loading frequency. This allows for a moderate power output over a greater duration compared to the large output over a short duration from the originally optimal realization.

6. CONCLUSIONS

The long-term deployment of a piezoelectric energy harvester, operating in near-resonant conditions, may lead to accumulated damage in the harvester. Subsequent shifts in the natural frequency may detune the harvester, affecting the harvester's power output. An investigation was performed to observe how damage accumulation affects the selection of tip mass and resistive load which maximize the power output of a piezoelectric bimorph. For the inputs considered, the following trends are noted:

- Degradation of the flexural rigidity leads to a reduction in the resonant frequency across all resistive loads. The reduced flexural rigidity results in a reduced optimal tip mass (for an unchanging input motion) and, since the power output is dependent on the tip mass, a reduced power output.
- Degredation of the piezoelectric terms does not significantly affect the tip mass corresponding to the maximum MRTD for low resistive loads but has some impact for high resistive loads. Degradation of the piezoelectric terms is concentrated in those tip mass realizations where the MRTD is high; in this study the realizations where the MRTD was high did not correspond to the realizations where the power output was high. Thus, degradation of the piezoelectric terms was not seen to significantly affect the maximum power output.

ACKNOWLEDGMENTS

This investigation was performed at the University of California San Diego as part of the first author's dissertation research. Funding was provided by Los Alamos National Laboratory through the Engineering Institute under Task 5 (Subcontract No. 77137-001-11). Neither the funding source nor Structural Integrity Associates, Inc. was involved with the study design; collection, analysis or interpretation of data; in the writing of the report; or in the decision to submit the article for publication.

REFERENCES

[1] Kjolsing, E. and Todd, M., "Damping of a fluid-conveying pipe surrounded by a viscous annulus fluid," Journal of Sound and Vibration 394, 575-592 (2017).
[2] Kjolsing, E. and Todd, M., "The impact of boundary conditions and fluid velocity on damping for a fluid conveying pipe in a viscous fluid," Proc. SPIE 9799, 979922 (2016).
[3] Kjolsing, E. and Todd, M., "Gauging the feasibility of a downhole energy harvesting system through a proof-of-concept study," Proc. SPIE 9799, 97992K (2016).
[4] Kjolsing, E. and Todd, M., "A frequency study of a clamped-clamped pipe immersed in a viscous fluid conveying internal steady flow for use in energy harvester development as applied to hydrocarbon production wells," Proc. SPIE 9435, 943505 (2015).
[5] Erturk, A. and Inman, D. J., [Piezoelectric Energy Harvesting], John Wiley & Sons, United Kingdom (2011).
[6] Priya, S. and Inman, D. J., [Energy Harvesting Technologies], Springer, New York (2009).
[7] Erturk, A. and Inman, D. J., "An experimentally validated bimorph cantilever model for piezoelectric energy harvesting from base excitations," Smart Materials and Structures 18(2), 025009 (2009).
[8] Erturk, A. and Inman, D. J., "A distributed parameter electromechanical model for cantilevered piezoelectric energy harvesters," Journal of Vibration and Acoustics 130(4), 041002 (2008).
[9] Miner, M. A., "Cumulative damage in fatigue," Journal of Applied Mechanics 12(3), 159-164 (1945).
[10] Nieslony, A., "Rainflow counting algorithm," MathWorks, 04 April 2010. http://www.mathworks.com/matlabcentral /fileexchange/3026-rainflow-counting-algorithm/content/index.html (10 June 2016).
[11] Nieslony, A., "Determination of fragments of multiaxial service loading strongly influencing the fatigue of machine components," Mechanical Systems and Signal Processing 23(8), 2712-2721 (2009).

FIGURES

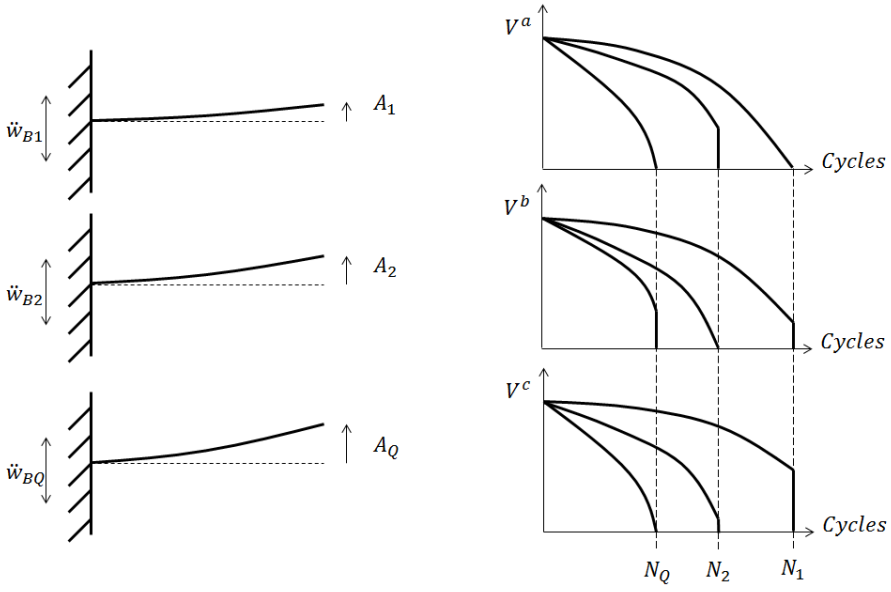

Figure 1. Cyclic testing of Q bimorphs.

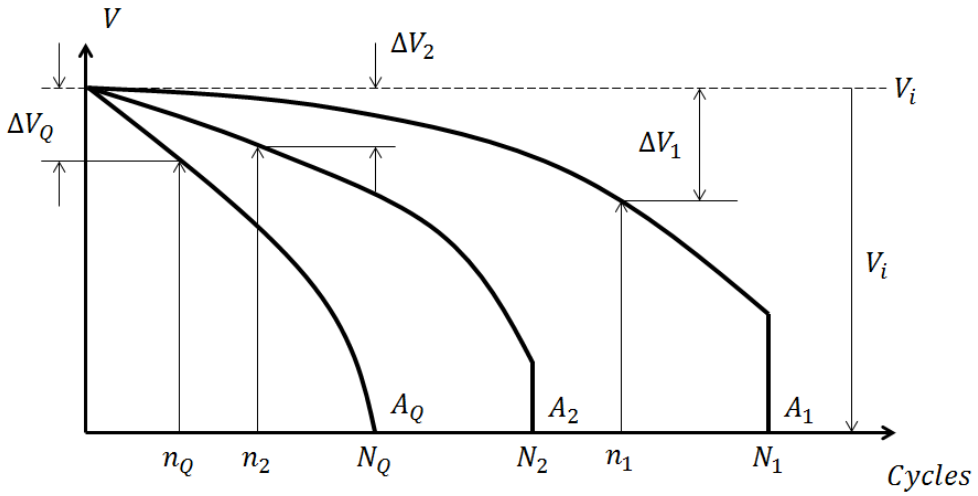

Figure 2. Cyclic degradation of property V at specific instant in time.

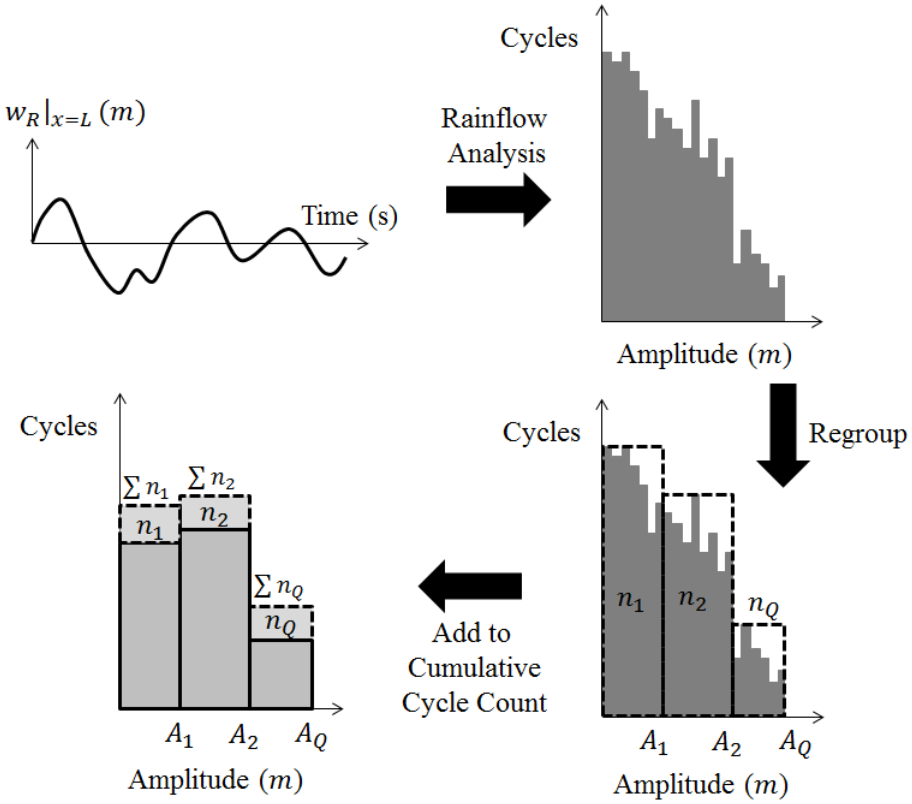

Figure 3. Regrouping rainflow output.

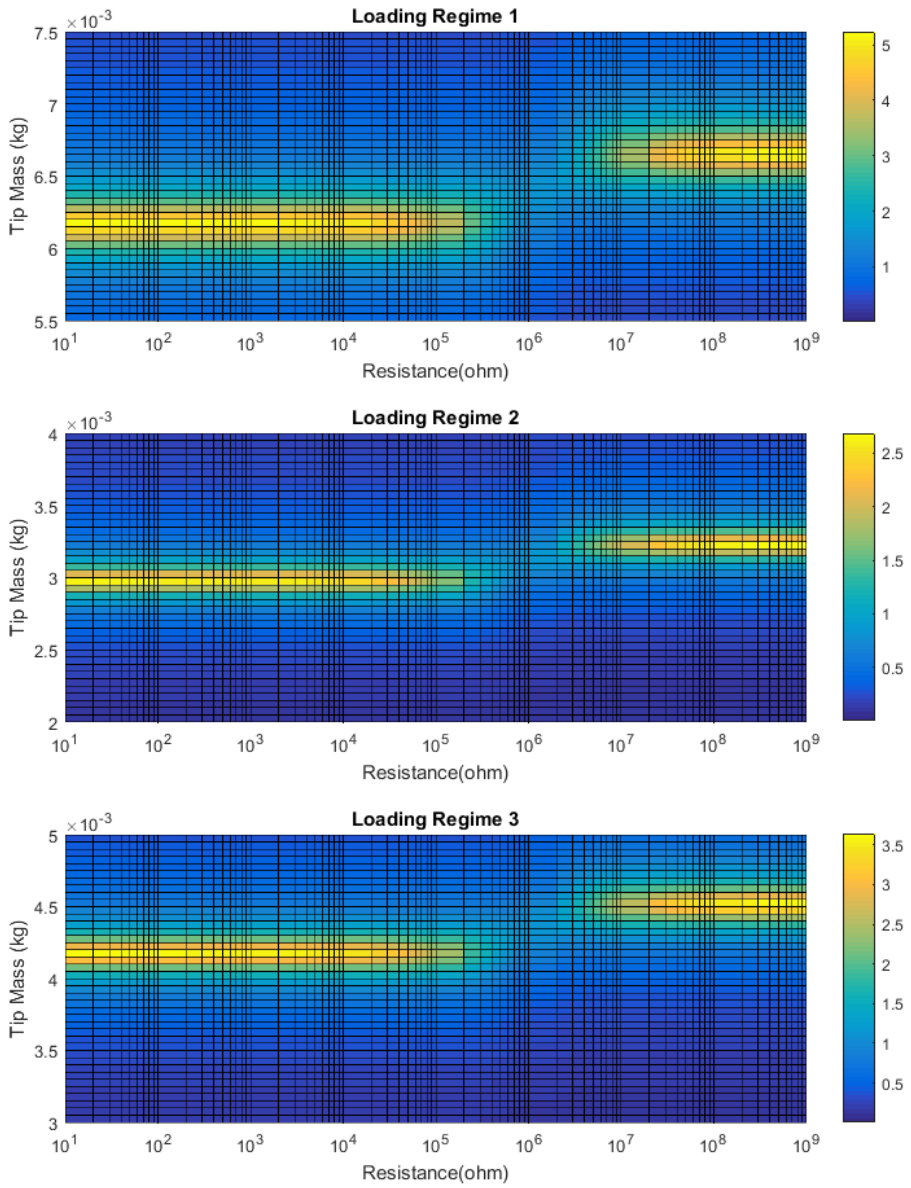

Figure 4. Maximum relative tip displacement (MRTD) (mm) contours: baseline case. Loading regime one (top), two (middle), and three (bottom) shown.

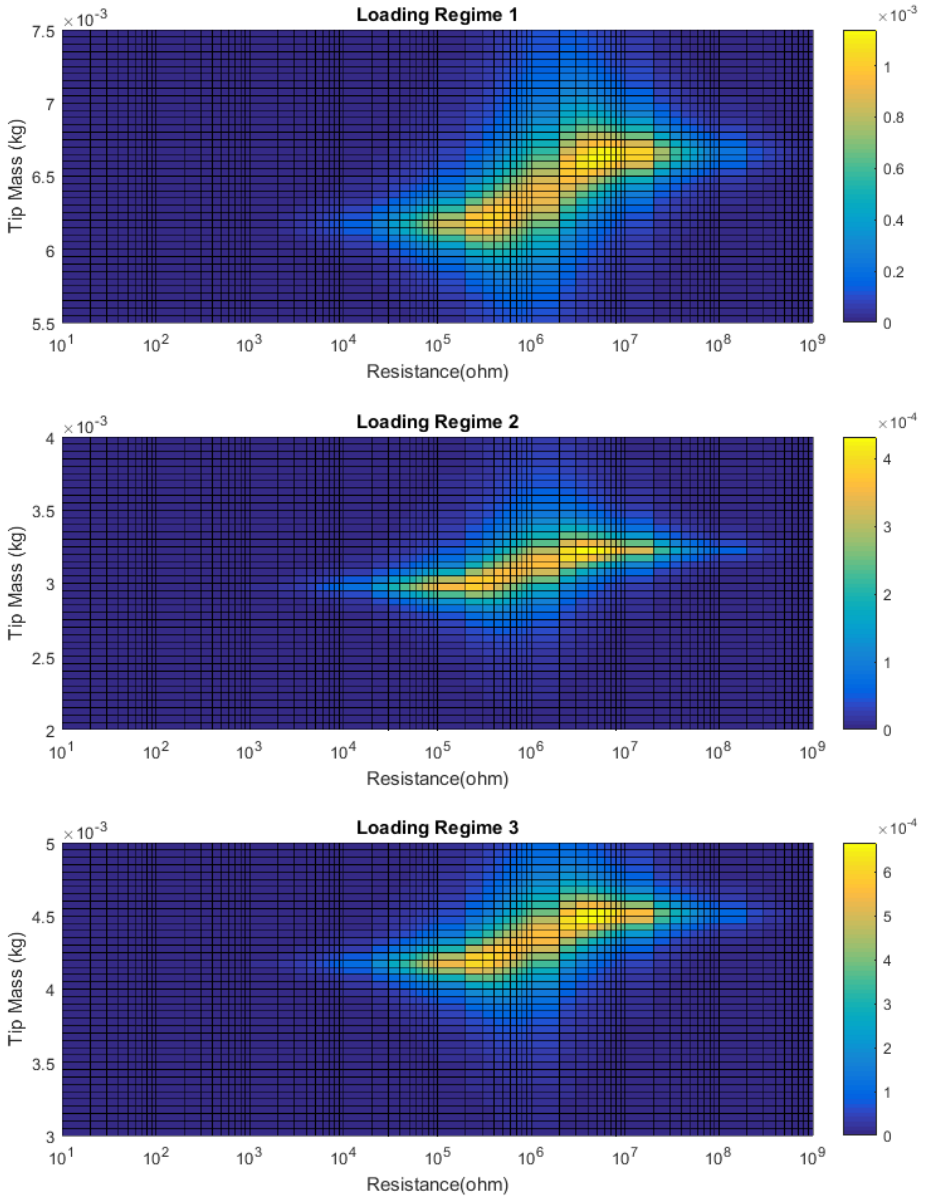

Figure 5. Average power (W) contours: baseline case. Loading regime one (top), two (middle), and three (bottom) shown.

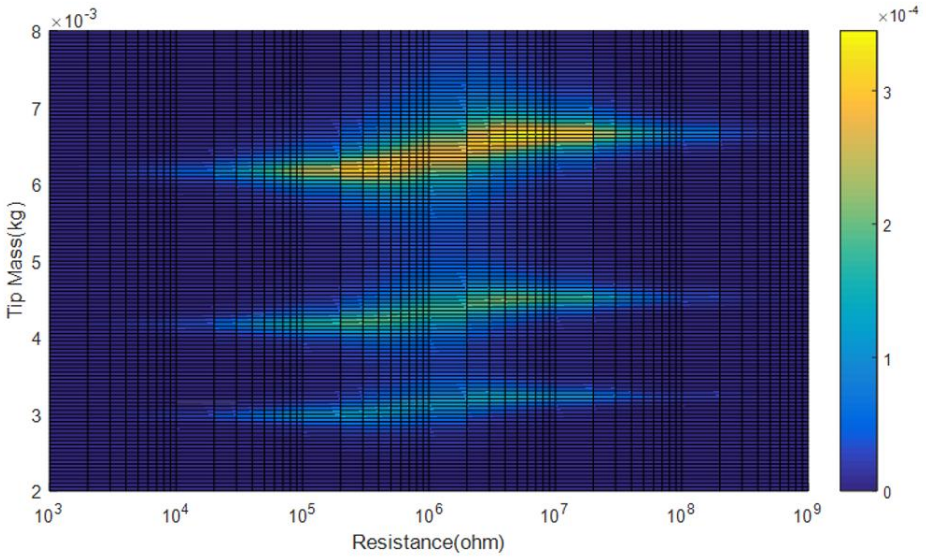

Figure 6. Integrated power metric (Wyr).

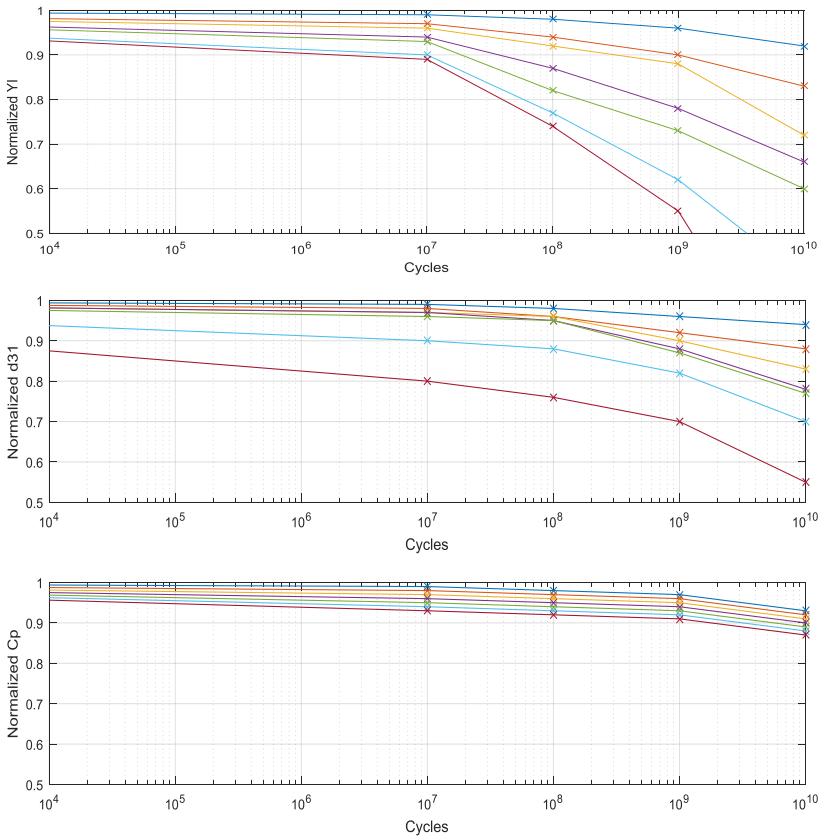

Figure 7. Normalized degradation of flexural and piezoelectric terms from cycling at specified amplitudes. $A_1 = 0.5mm$ (blue), $A_2 = 1mm$ (orange), $A_3 = 1.5mm$ (yellow), $A_4 = 2mm$ (purple), $A_5 = 3mm$ (green), $A_6 = 5mm$ (cyan), $A_7 = 7mm$ (red).

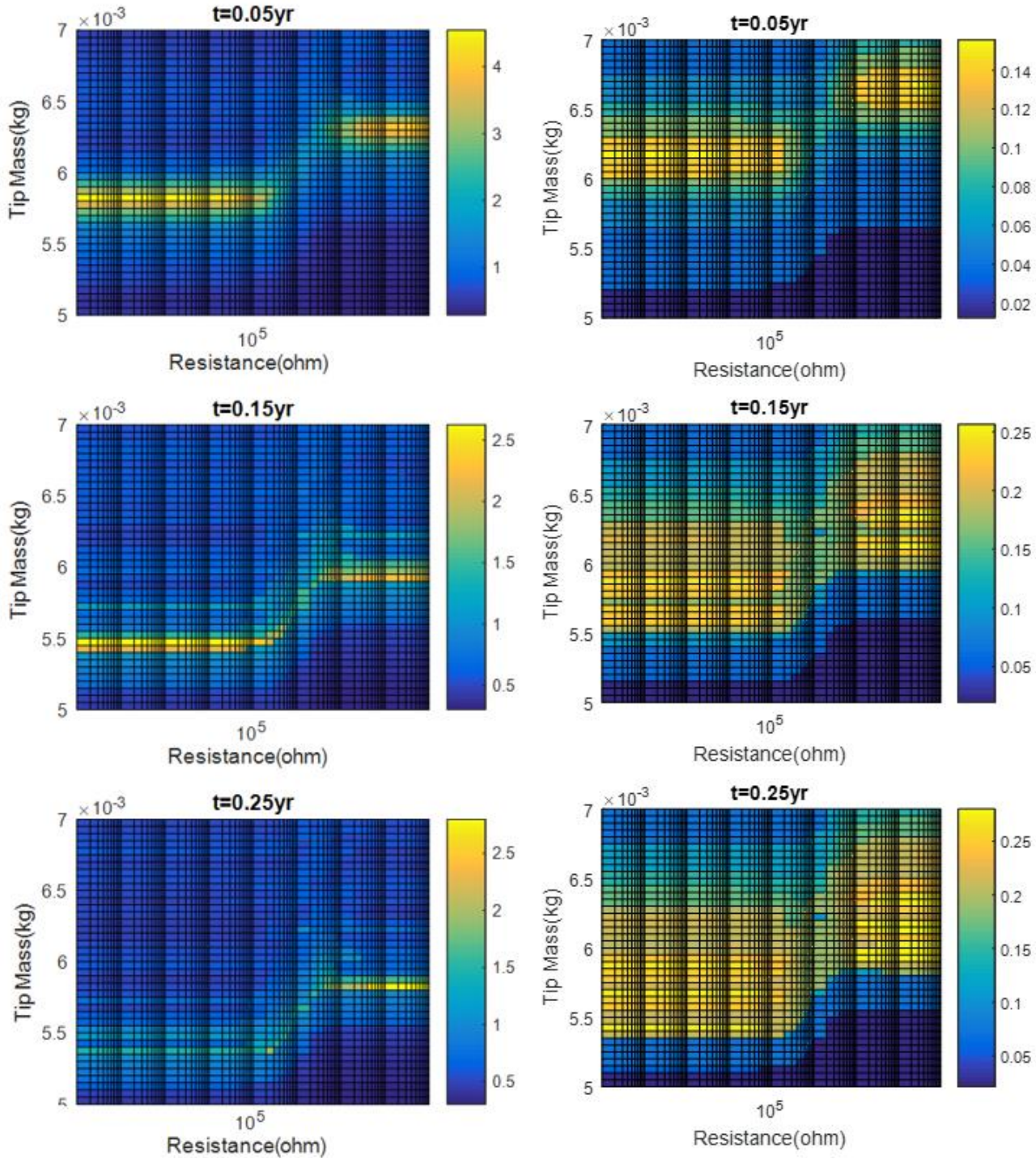

Figure 8. Maximum relative tip displacement (MRTD) (mm; left) and cumulative damage (C; right) contours based on degradation of flexural rigidity. Results applicable for $0.05yr$ from the initial time indicated.

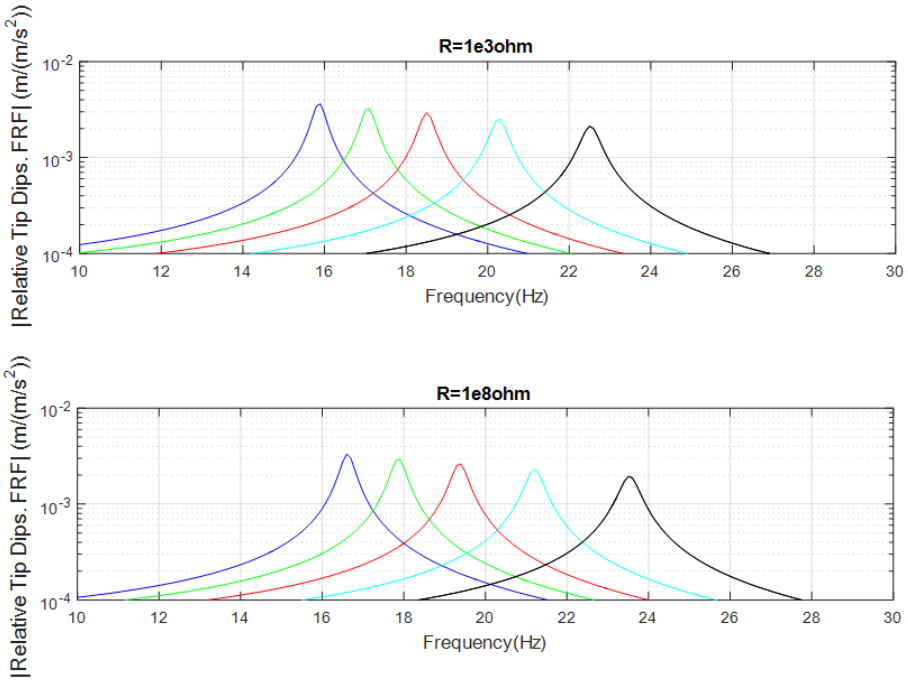

Figure 9. Relative tip displacement FRFs for various resistive loads and tip masses. $0.009kg$ (blue), $0.008kg$ (green), $0.007kg$ (red), $0.006kg$ (cyan), $0.005kg$ (black).

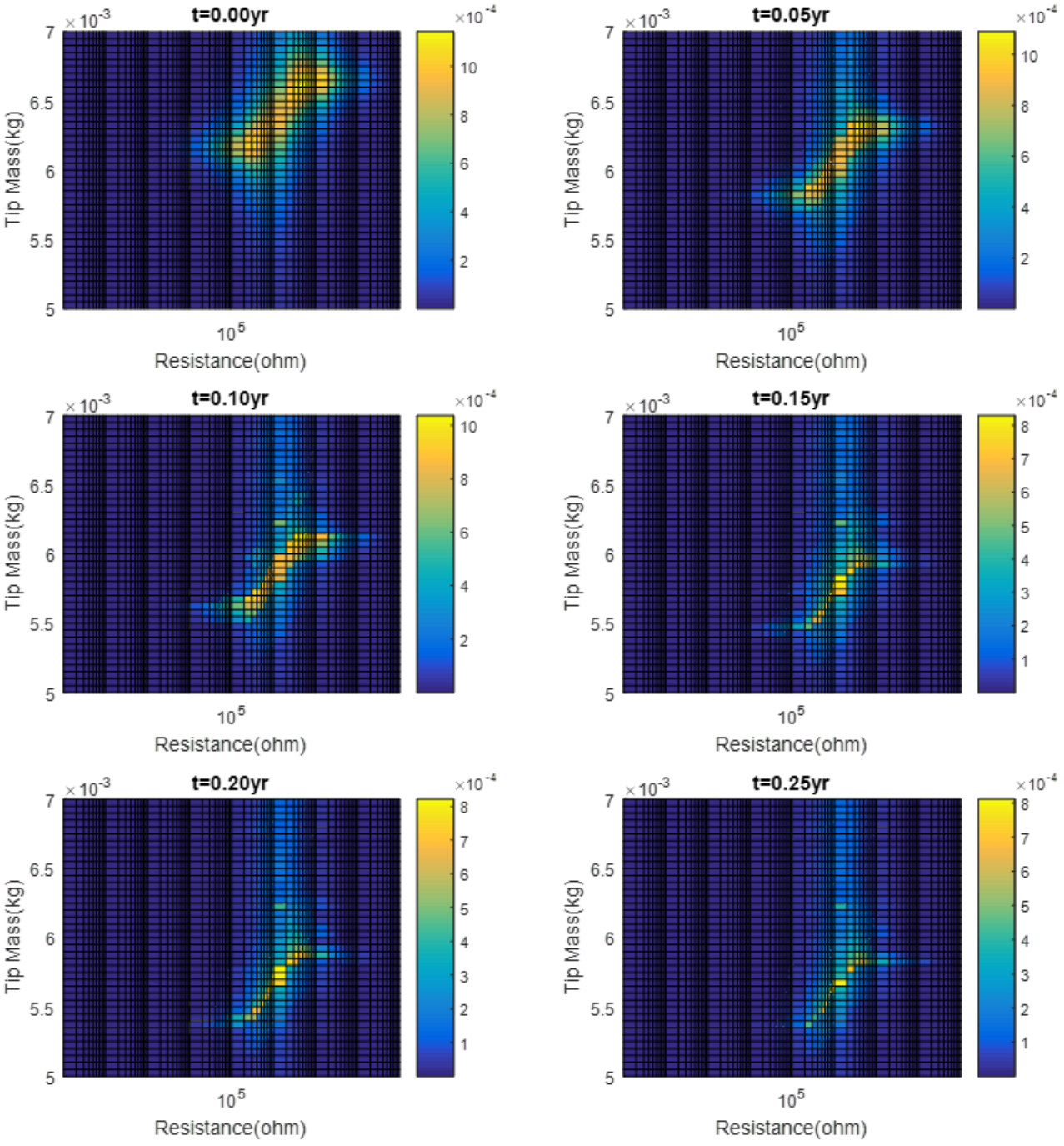

Figure 10. Average power (W) contours based on degradation of flexural rigidity. Results applicable for $0.05yr$ from the initial time indicated.

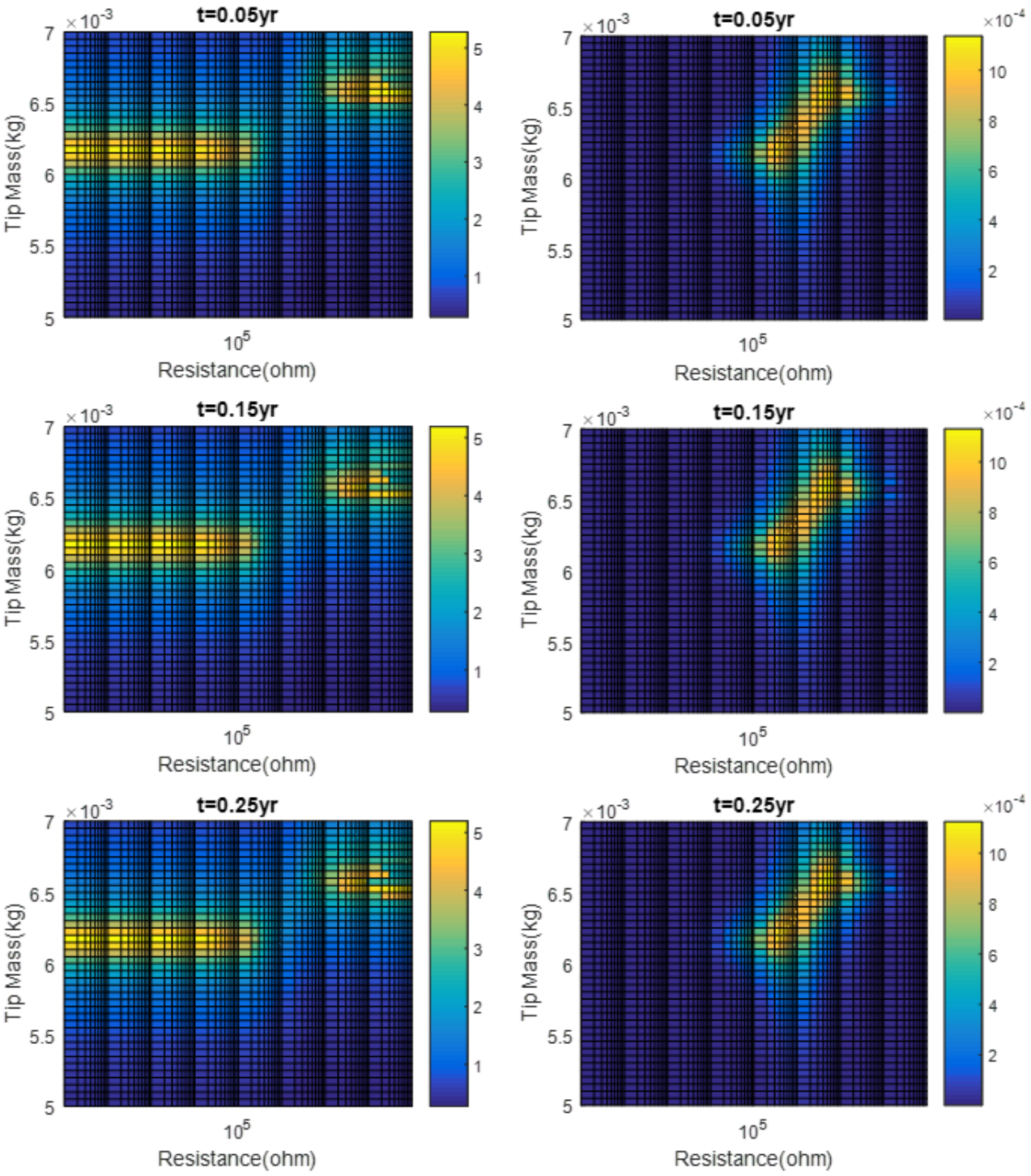

Figure 11. Maximum relative tip displacement (MRTD) (mm; left) and average power (W; right) contours based on degradation of piezoelectric terms. Results applicable for $0.05yr$ from the initial time indicated.

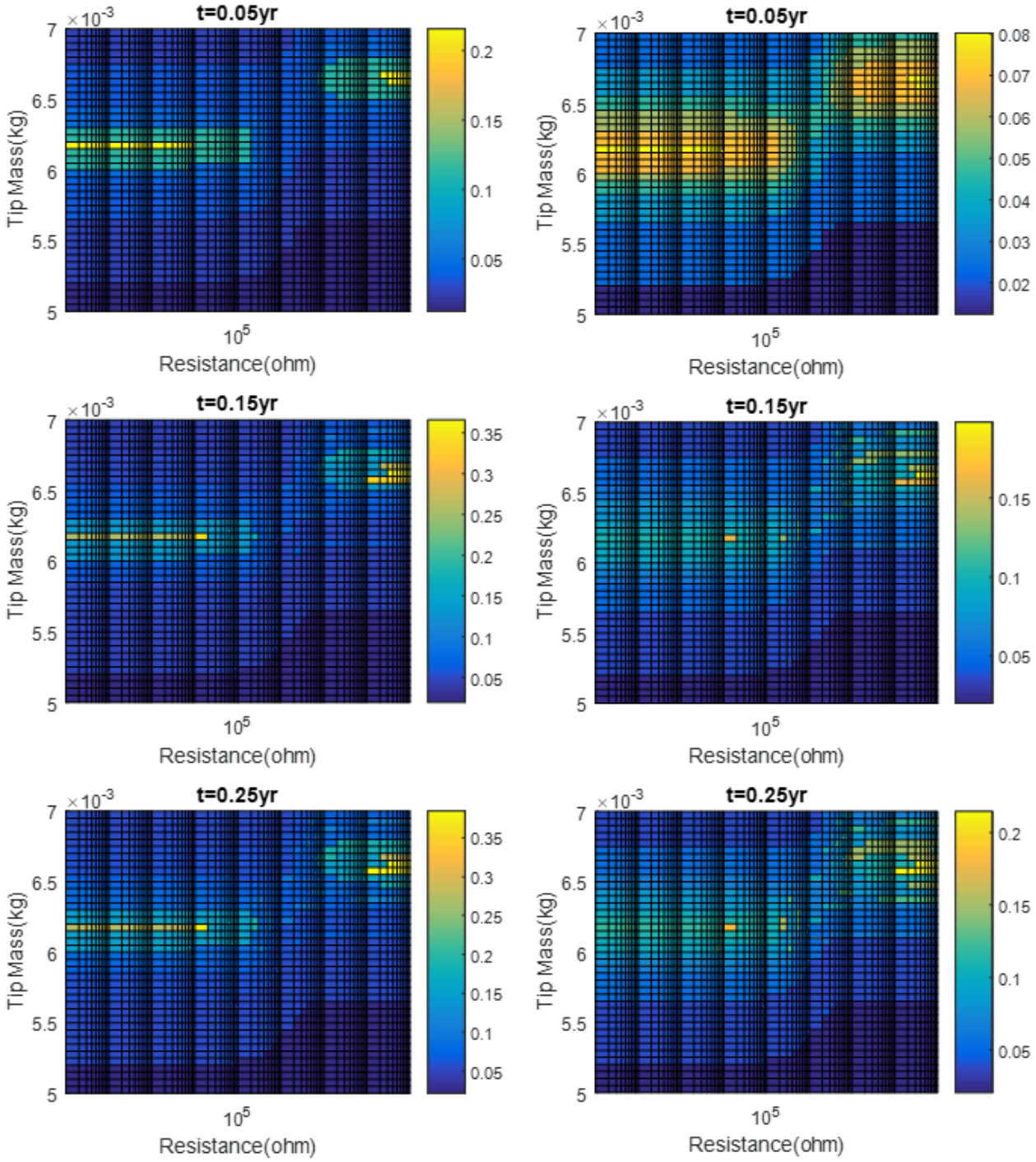

Figure 12. Cumulative damage (C) contours of d_{31} (left) and $C_{\tilde{p}}$ (right) based on degradation of piezoelectric terms. Results applicable for $0.05yr$ from the initial time indicated.

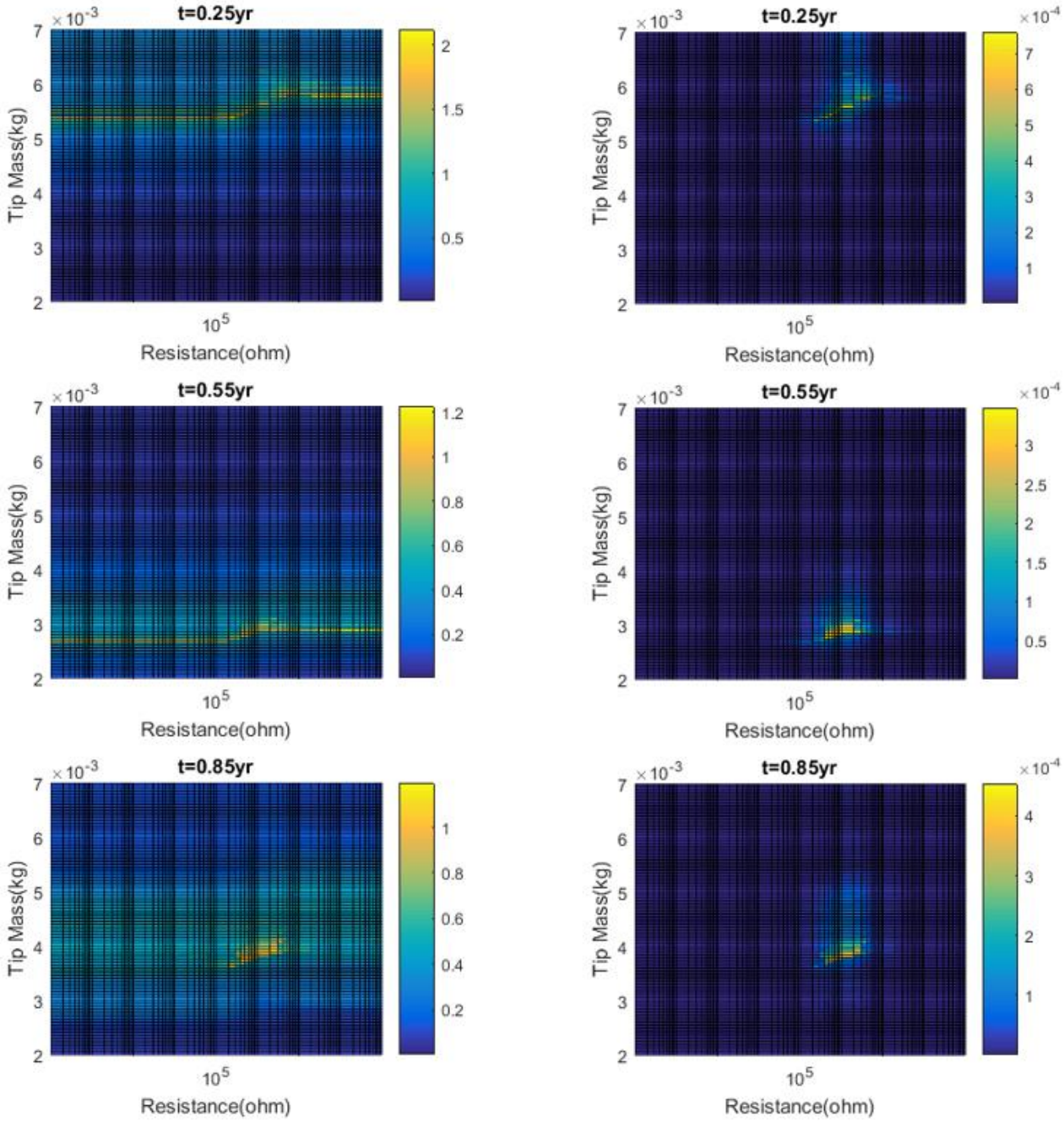

Figure 13. Maximum relative tip displacement (MRTD) (mm; left) and average power (W; right) contours based on full degradation model. Results applicable for $0.05yr$ from the initial time indicated.

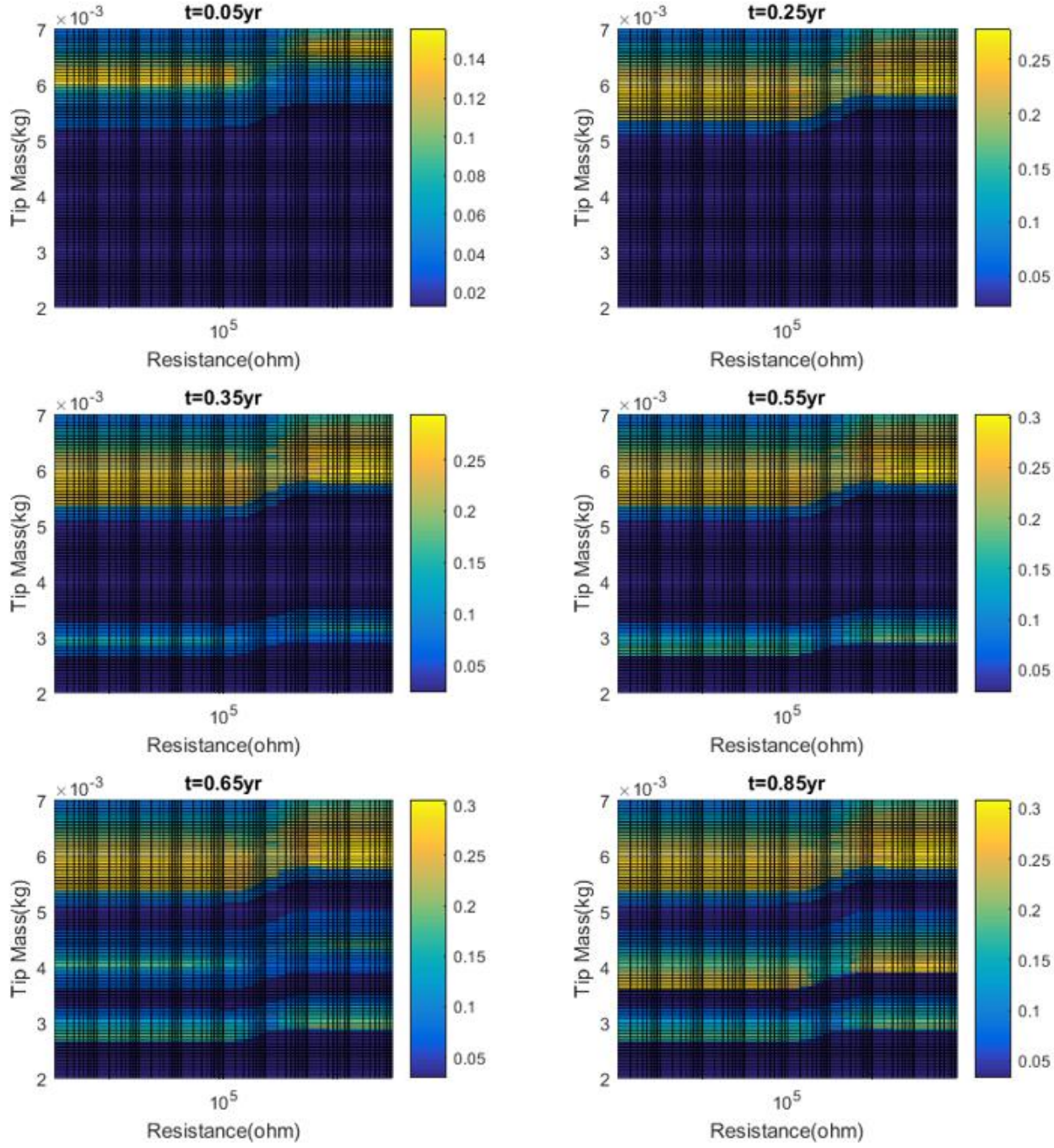

Figure 14. Cumulative damage (C) contours of flexural rigidity based on full degradation model. Results applicable for $0.05yr$ from the initial time indicated.

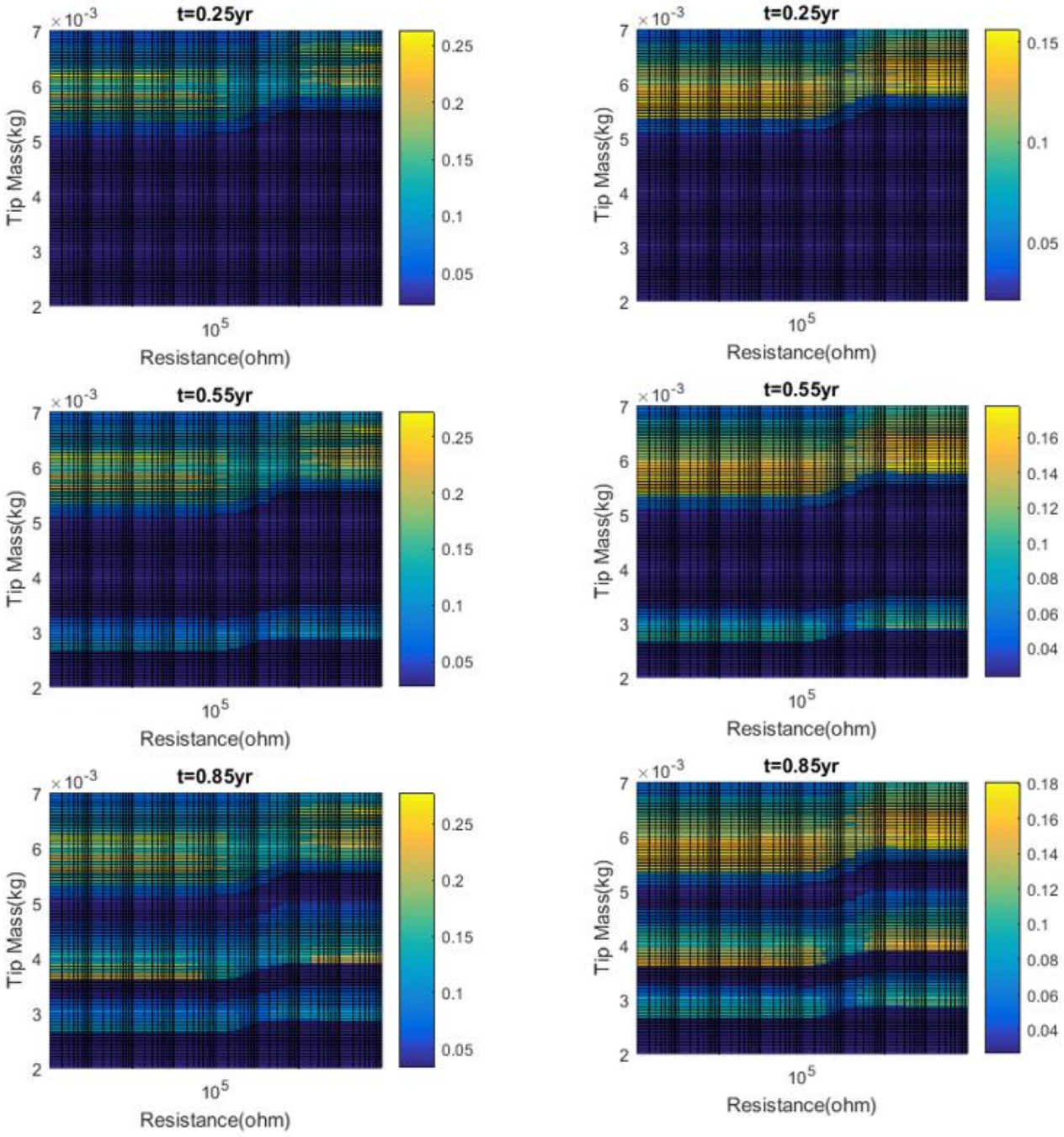

Figure 15. Cumulative damage (C) contours of d_{31} (left) and $C_{\tilde{p}}$ (right) based on full degradation model. Results applicable for $0.05yr$ from the initial time indicated.

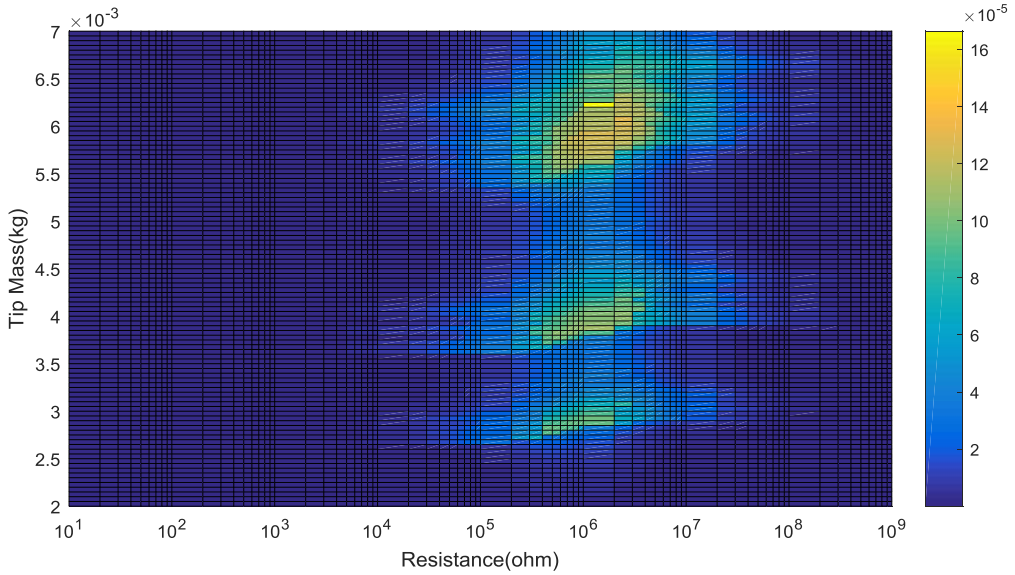

Figure 16. Integrated power metric (Wyr).

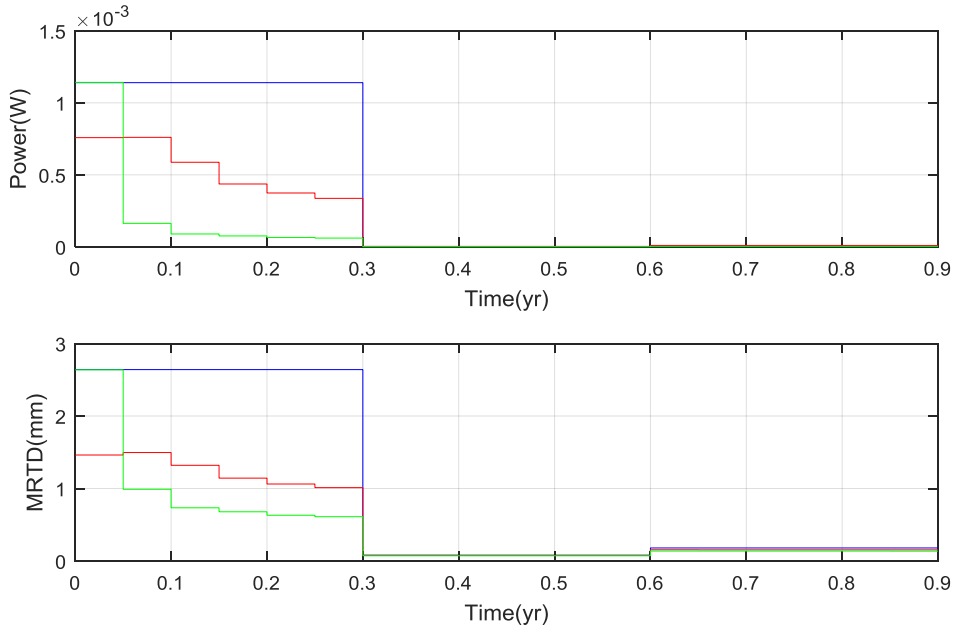

Figure 17. Average power output and maximum relative tip displacement (MRTD). $M_t = 0.0066kg$, $R = 5e6\Omega$ with no damage (baseline; blue). $M_t = 0.0066kg$, $R = 5e6\Omega$ with damage (green). $M_t = 0.0062kg$, $R = 1e6\Omega$ with damage (new optimum; red).